

## 250-GHz EPR of Nitroxides in the Slow-Motional Regime: Models of Rotational Diffusion

Keith A. Earle, David E. Budil, and Jack H. Freed\*

Baker Laboratory of Chemistry, Cornell University, Ithaca, New York 14853

Received: July 27, 1993\*

A 250-GHz electron paramagnetic resonance (EPR) study of the slow rotational diffusion of two spin probes in toluene, viz., perdeuterated 2,2,6,6-tetramethyl-4-piperidone (PDT) and 3-doxylcholestane (CSL) is presented. EPR spectra were obtained in the slow-motional and near-rigid limit regions, which corresponds to rotational correlation times  $10^{-10} > \tau_R > 10^{-6}$  s. These two probes differ significantly in size and shape, permitting a detailed exploration of the sensitivity of 250-GHz EPR to different aspects of the molecular dynamics such as rotational anisotropy and non-Brownian diffusion. Nonlinear least-squares fitting based on full stochastic Liouville calculations provides a sensitive means for discriminating amongst motional models. PDT in toluene- $d_6$  is found to be well described by an approximate free diffusion model, whereas the larger spin probe, CSL, is best described by Brownian diffusion. The slow-motional spectra at 250 GHz are most sensitive to the diffusional model, the (geometric) mean diffusional rate, and axial diffusional anisotropy but less sensitive to rhombic deviations from an axially symmetric diffusion tensor (i.e., to the general case  $R_x \neq R_y \neq R_z$ ). The slow-motional spectra of PDT were fit using anisotropic diffusion parameters determined from fast-motional spectra but are not very sensitive to such small anisotropies. For the case of Brownian diffusion, CSL was best fit with  $N_y \equiv R_y/(R_x R_z)^{1/2} = 9.0$  (where the  $y$  axis is the long axis of the molecule and  $x$  and  $z$  are perpendicular axes), which differs appreciably from the fast-motional value of  $N_y = 4.3 \pm 0.2$  (and  $\rho_x \equiv R_x/R_z = 0.5$ ). However, a mixed model of free-diffusional motion about the  $y$  axis with Brownian motion of this axis yields an  $N_y$  close to the fast-motional value with comparable overall quality in fit compared to full Brownian motion. An important feature of the 250-GHz studies is the ability to measure very accurately the magnetic tensors needed for the motional studies. The theoretical modifications needed for inclusion of a fully anisotropic rotational diffusion tensor in the slow-motional EPR simulations are also given.

### Introduction

Electron paramagnetic resonance (EPR) has been an invaluable tool for probing microscopic molecular motions in a variety of systems, including isotropic solvents,<sup>1–3</sup> liquid crystals,<sup>4,5</sup> model membranes,<sup>6,7</sup> and biomolecules.<sup>7</sup> The EPR spectrum of a radical depends not only on the magnetic interactions of the unpaired electron spin but also on the reorientational motion of the probe molecule. The dependence is relatively simple when the reorientation is sufficiently fast, or more specifically, when  $\tau_R \Delta\omega \ll 1$ , where  $\tau_R$  is the correlation time characterizing the motion and  $\Delta\omega$  is a measure of the magnitude of the orientation-dependent part of the spin Hamiltonian. In this case the EPR spectrum is a simple superposition of Lorentzian lines whose widths may be related to  $\tau_R$  by motional narrowing theory after accounting for inhomogeneous broadening.

For slower rotations, i.e., when  $\tau_R \Delta\omega \geq 1$ , the EPR spectrum depends in a much more complicated fashion on the combined influences of molecular motion and magnetic interactions, and the line shape can be fully analyzed only by using a theoretical approach incorporating a detailed description of the molecular motions.<sup>5,8</sup> These “slow-motional” line shapes are most often calculated using the stochastic Liouville equation, which can be solved numerically<sup>9</sup> to obtain the EPR spectra for arbitrarily fast or slow motions and for various Markovian models for reorientation. Thus, the slow-motional EPR line shape, in principle, provides a more detailed picture of the molecular dynamics, at some sacrifice in the simplicity of the analysis.

At conventional EPR frequencies of 9–35 GHz, rotational dynamics in most fluids occurs on the fast-motional time scale, which limits the amount of detailed information that can be obtained. This constraint has motivated the extension of molecular dynamics studies by EPR to superconducting magnet fields requiring resonant radiation at wavelengths on the order of  $\lambda =$

1–2 mm, corresponding to frequencies above 140 GHz.<sup>10–12</sup> Because of the greatly increased  $\Delta\omega$  at such frequencies, rotational motions typically encountered in condensed phases are more likely to fall into the slow-motional regime, thereby permitting a much more detailed analysis. Another important feature of such high-frequency studies is the enhanced accuracy with which the components of the  $g$  and  $A$  tensors may be determined from rigid-limit spectra obtained at 250 GHz. In fact the high resolution to slow motions at this frequency is largely due to the enhanced  $g$ -factor resolution, so the regions of the spectrum corresponding to magnetic  $x$ ,  $y$ , and  $z$  are clearly discerned. Thus, the line positions and widths associated with each of these three canonical orientations, as well as the line shapes between them, provide sensitive criteria for discriminating amongst various models for rotational diffusion.

The advantages of studying slow motions at high EPR fields are offset somewhat by the increased computational challenge of carrying out a rigorous analysis. In particular, the increased spectral resolution, as well as the larger  $\Delta\omega$  of the high-field spectra, requires correspondingly larger basis sets in the eigenfunction expansion of the stochastic Liouville equation needed to calculate the EPR spectrum. Until recently, the computer time needed to carry out a single high-field slow-motional calculation was so substantial that it restricted the fitting of spectra, which typically requires large numbers of simulations as one iterates to a good fit.

Powerful and efficient computational methods were required for generating accurate spectral simulations of the entire line shape in the model-sensitive region. We have developed a computational package, which combines the full stochastic Liouville spectral calculation<sup>9</sup> with an accurate nonlinear least-squares analysis that is very efficient.<sup>13</sup> It has enabled us to study the 250-GHz line shapes in detail.

As an application of the highly resolved 250-GHz EPR spectra and our enhanced fitting capabilities, we present a study of the

\* Abstract published in *Advance ACS Abstracts*, November 15, 1993.

slow rotational diffusion of two spin probes in toluene, viz., perdeuterated 2,2,6,6-tetramethyl-4-piperidone (PDT) and 3-doxylcholestanol (CSL). The two spin probes have very different shapes and sizes: whereas PDT is relatively small and nearly spherical in shape, CSL is larger and cigar-shaped. These differences permit a detailed exploration of the effects of rotational anisotropy and motional model on 250-GHz EPR spectra. For example, the motion of CSL should be much more anisotropic than that of PDT, and CSL is more likely to exhibit Brownian diffusion. In contrast, the assumptions leading to a Brownian diffusional model may break down for the smaller probe, PDT, which is comparable in size to the solvent molecules.

We find that the temperature dependence of the slow-motional EPR line shapes at 250 GHz is rather different for these two probes, and in the process we demonstrate the high sensitivity of this method both to the specific model for rotational diffusion of the molecule and to its rotational anisotropy.

### Experimental Section

EPR spectra of the perdeuterated spin probe 2,2,6,6-tetramethyl-4-piperidone (PDT) in toluene- $d_8$  and 3-doxylcholestanol spin label (CSL) in toluene were measured at 250 GHz as a function of temperature in the range  $-70$  to  $-136$  °C, which includes all of the slow-motional regime at 250 GHz for both spin probes. Supplemental measurements were also performed at 9.5 GHz over a more limited temperature range. The 250-GHz EPR spectrometer and its operation have been described previously.<sup>12,14</sup> Toluene- $d_8$  (99.95% D) was obtained from Aldrich Chemical Company and used without further purification other than drying over molecular sieves. The PDT was synthesized locally according to published procedures<sup>2</sup> and purified by vacuum sublimation. The CSL was obtained from Sigma Chemical Company and used without further purification. Stock solutions of each probe were prepared by dissolving a weighed amount of the probe with overnight stirring at room temperature; sample aliquots were diluted to final concentrations of 0.5 mM (for PDT) and 1.0 mM (for CSL) in order to minimize the line width due to Heisenberg exchange. The samples were degassed under vacuum and sealed in 6 mm o.d. quartz tubes. Before line-shape analysis, the phases of the experimental spectra were adjusted to correct for a slight admixture of dispersion signal that results from small misalignments of the detector wave guide from the plane of polarization of the incident radiation. The phase correction was accomplished by taking a linear combination of the measured signal and a calculated quadrature signal (generated from the Hilbert transform of the measured signal) and adjusting the admixture of both components across the spectrum until the integrated combination spectrum displayed a flat, zero base line. We have also obtained a usable quadrature signal by measuring the spectrum at a different detector orientation and combining the spectra from the two detector orientations, although that method was not employed in this work.

### Results

**Magnetic Parameters.** In order to characterize the motional parameters of the probes, it is first necessary to have accurate magnetic tensor parameters. Figure 1 shows a near rigid limit spectrum of CSL obtained at about  $-123$  °C. (Rigid-limit parameters for PDT in toluene- $d_8$  have been obtained previously.<sup>20</sup>) The  $g$  and  $A$  magnetic tensors were obtained by least-squares spectral simulation and are given in Table I. For CSL, the spectrum obtained at the coldest temperature still exhibited some small effects of residual motion. This spectrum was therefore simulated using the slow-motional line-shape program with a rotational correlation time of about  $10^{-6}$  s. For such correlation times, which are very near the rigid limit for 250 GHz, different models for rotational diffusion give nearly identical peak positions (although the spectra do differ in the details of the line shape as

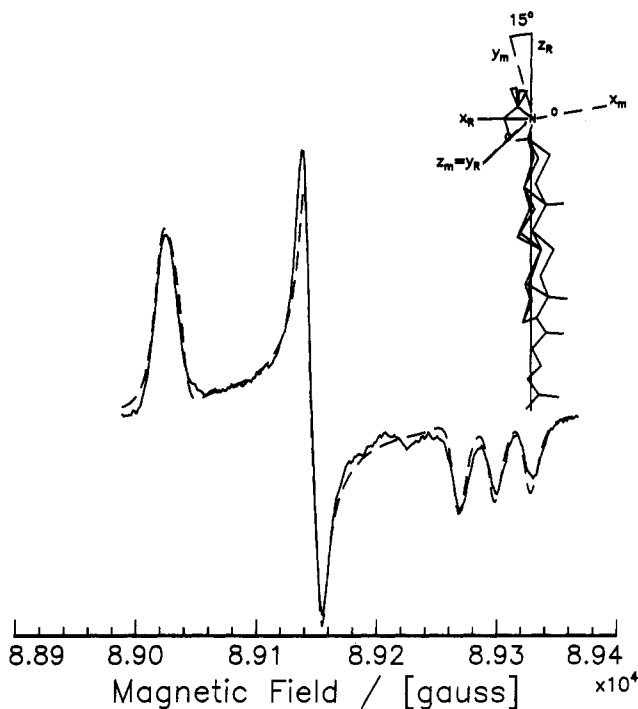


Figure 1. 250-GHz rigid-limit spectrum of CSL in toluene (solid line) and least-squares simulation (dashed line). The magnetic tensor parameters used in the simulation are given in Table I. Inset shows the magnetic axes ( $x_m$ ,  $y_m$ , and  $z_m$ ) and the diffusion axes ( $x_R$ ,  $y_R$ ,  $z_R$ ) relative to the molecular frame of CSL including a  $15^\circ$  diffusion tilt angle.

TABLE I: Magnetic Parameters Measured from Rigid-Limit Samples of PDT in Toluene- $d_8$  and CSL in Toluene at 250 GHz

	PDT <sup>a</sup>	CSL <sup>b</sup>
$g_x$	$2.00936 \pm 3 \times 10^{-5}{}^c$	$2.00855 \pm 3 \times 10^{-5}{}^c$
$g_y$	$2.00633 \pm 3 \times 10^{-5}{}^c$	$2.00574 \pm 3 \times 10^{-5}{}^c$
$g_z$	$2.00233 \pm 3 \times 10^{-5}{}^c$	$2.00221 \pm 3 \times 10^{-5}{}^c$
$\langle g \rangle^d$	$2.00601 \pm 5 \times 10^{-5}$	$2.00550 \pm 5 \times 10^{-5}$
$g_s^e$	$2.00602^f$	$2.00553^g$
$A_x/\gamma_e$	$4.1 \pm 0.2$	$7.1 \pm 0.2$
$A_y/\gamma_e$	$5.1 \pm 0.2$	$4.5 \pm 0.2$
$A_z/\gamma_e$	$33.6 \pm 0.2$	$30.2 \pm 0.4$
$\langle A \rangle/\gamma_e^h$	$14.3 \pm 0.3$	$13.9 \pm 0.5$
$\alpha_N^i$	$14.3 \pm 0.2$	$13.8 \pm 0.1$
$\beta_d^j$	$0^\circ$	$15^\circ$

<sup>a</sup> Reference 20. <sup>b</sup> This work. <sup>c</sup> This absolute error is dominated by the field calibration error; the relative error (i.e., the error in  $g_i$  relative to a calibration point in the spectrum) is estimated from the spectral fits to be  $5 \times 10^{-6}$  for PDT and  $7 \times 10^{-6}$  for CSL. <sup>d</sup>  $\langle g \rangle = (g_x + g_y + g_z)/3$ . <sup>e</sup> Measured in motionally narrowed region. <sup>f</sup> Calibrated to  $g_s$  measured for 0.1 mM PDT in toluene- $d_8$  at X-band, from ref 2. <sup>g</sup> Calibrated to  $g_s$  measured for 1.0 mM CSL in toluene at 9.5 GHz. <sup>h</sup>  $\langle A \rangle = (A_x + A_y + A_z)/3$ . <sup>i</sup> Not determined from fits; value for CSL derived from molecular model.<sup>15</sup>

discussed below) and therefore provide a reasonably reliable estimate of the magnetic tensors. Because of the residual motion and also the increased inhomogeneous line width due to superhyperfine (shf) interactions with the protons on CSL, the magnetic parameters were determined to slightly less accuracy than those for PDT; nevertheless, they were sufficiently accurate for the analysis of the slow-motional spectra throughout the temperature range studied.

The  $g$  and  $A$  tensors obtained at 250 GHz for CSL in toluene are significantly more rhombic in character than the tensor parameters that have been determined for CSL in liquid crystalline media<sup>15</sup> at 9.5 GHz. In Table I we show the magnetic tensor parameters for PDT in toluene- $d_8$  determined previously, as well as the parameters for CSL in toluene determined in this work.

**Fast-Motional Data Analysis for CSL.** For the CSL spectra falling into the fast-motional regime (above about  $-60$  °C) we

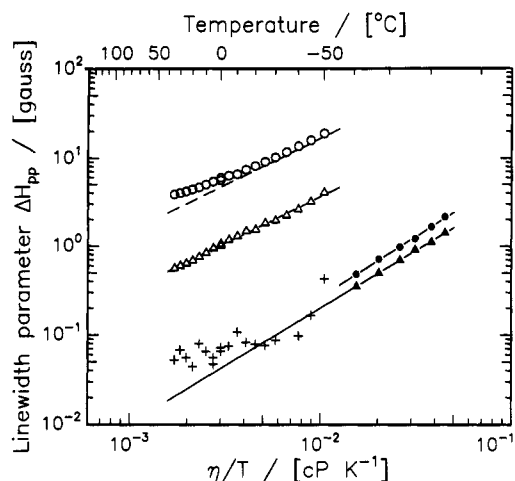


**Figure 2.** Fast-motional line width parameters for CSL in toluene measured at 250 and 9.5 GHz as a function of temperature: (O)  $A_{250}$ , ( $\Delta$ )  $B_{250}$ , (+)  $C_{250}$ , ( $\bullet$ )  $B_{9.5}$ , and ( $\blacktriangle$ )  $C_{9.5}$ . The spacing between the least-squares lines shown for  $B_{9.5}$  and  $C_{9.5}$  corresponds to a  $C_{9.5}/B_{9.5}$  ratio of 1.50. The dashed line for  $A_{250}$  corresponds to a constant  $A_{250}/B_{250}$  ratio of 4.6 relative to the least-squares line for  $B_{250}$ ; the residual inhomogeneous line width of 0.9 G is apparent as a deviation of  $A_{250}$  from linearity.

used a method described previously<sup>20</sup> to derive accurate values for the rotational anisotropy parameters  $\rho_x \equiv R_x/R_z$  and  $\rho_y \equiv R_y/R_z$  (where the  $x$ ,  $y$ , and  $z$  coordinates refer to the  $x_m$ ,  $y_m$ , and  $z_m$  axes of the magnetic tensor given in Table I). The three resolved lines that appear in the 250-GHz spectrum in this temperature range are very well approximated by Lorentzian line shapes. The derivative peak-to-peak width of each  $m_l$  line was determined by fitting the sum of three (first-derivative) Lorentzian functions to the experimental spectrum, and the line widths thus derived were used to calculate the parameters  $A$ ,  $B$ , and  $C$  using the equation  $\Delta H_{pp}(m_l) = A + Bm_l + Cm_l^2$ . Figure 2 shows a plot of the experimental  $A$ ,  $B$ , and  $C$  parameters as a function of  $\eta/T$ , using an empirical formula for the viscosity  $\eta(T)$  of toluene and toluene- $d_8$  given by Barlow *et al.*<sup>16</sup> and Zager.<sup>17</sup>

At the highest temperatures studied, the  $A$  term exhibited noticeable effects of inhomogeneous broadening due to super-hyperfine splittings (shfs) of the protons on the CSL probe. This inhomogeneity is apparent as a deviation from linearity in the plotted  $A$  parameter shown in Figure 2 at  $\eta/T$  values below about  $5 \times 10^{-2}$ , corresponding to temperatures above  $-10$  °C. At lower temperatures, however, the  $A/B$  ratio was constant at  $4.6 \pm 0.1$ .

As Figure 2 also shows, there is a significant amount of scatter in the experimental  $C$  parameter measured at 250 GHz. In principle, given sufficient signal-to-noise to determine  $C$  accurately, it should be possible to use both the  $A/B$  and  $C/B$  ratios measured in the low-temperature region at 250 GHz to determine  $\rho_x$  and  $\rho_y$ .<sup>20</sup> In practice, however, at 250 GHz  $C$  is the small difference of large line widths, which results in large relative errors. To circumvent this weakness, we measured  $B$  and  $C$  at 9.5 GHz. However, the line shape of the individual  $^{14}\text{N}$  hyperfine lines at 9.5 GHz suffers much more significantly from inhomogeneous broadening than at 250 GHz. This is because the homogeneous broadening associated with the rotational motion is much greater at 250 GHz and therefore constitutes a larger fraction of the total width. In fact, the shf interactions with the protons of CSL are resolvable over much of the temperature range studied at 9.5 GHz. Under these conditions, it is quite difficult to measure  $B$  and  $C$  accurately. Below temperatures of about  $-70$  °C, however, the shfs is no longer resolvable, and it was possible to determine the line-width parameters with reasonable accuracy using the methods described by Bales<sup>18</sup> to account for the inhomogeneous line width. (At 250 GHz the inhomogeneity is such a small contribution to the overall line

width that this procedure was not needed.) The  $C$  and  $B$  data measured at 9.5 are also shown in Figure 2. These data give a  $C/B$  ratio of  $1.50 \pm 0.05$ . Using the method of solving two linear allowed-value equations (AVEs)<sup>19,20</sup> based on the  $A/B$  ratio measured at 250 GHz and the  $C/B$  ratio measured at 9.5 GHz (as well as the magnetic parameters defined in Table I), we found  $\rho_y = 3.0 \pm 0.2$  and  $\rho_x = 0.5 \pm 0.2$ . These results indicate that the axis of the fastest rotation is the  $y$  magnetic axis, which corresponds most closely to the long axis of the cholestane moiety (defined as the  $z$  axis of the rotational diffusion tensor). This result is consistent with previous studies of CSL in liquid crystals<sup>15</sup> and model membranes,<sup>21,22</sup> as well as molecular models which show that the  $z$  diffusion axis lies approximately  $15^\circ$  away from the magnetic  $y$  axis.<sup>15</sup> The coordinate systems for the magnetic tensor ( $x_m, y_m, z_m$ ) and diffusion tensor ( $x_R, y_R, z_R$ ) of CSL used in this work are shown in the inset in Figure 1. (Note that we considered the effects of this small tilt of the two axis systems on the analysis and we found that it hardly affected the fast-motional analysis, cf. discussion below.)

**Slow-Motional Data Analysis.** To determine the motional parameters of PDT and CSL from the experimental spectra in the slow-motional regime, we performed nonlinear least-square fits to the experimental spectra shown in Figure 3 parts a, b, and c. The fitting procedure was carried out using program NLSL,<sup>13</sup> a nonlinear least-squares fitting procedure based on an updated version of the published EPRLL line-shape programs<sup>9</sup> and a revision of the modified Levenberg–Marquardt algorithm available in the MINPACK subroutine library.<sup>23</sup>

As discussed above, the fast-motional line widths obtained for both PDT and CSL at 250 GHz permit a full determination of the rotational diffusion tensor anisotropy.<sup>20</sup> In order to check the sensitivity of slow-motional line shapes at 250 GHz to rotational anisotropy, we have modified the slow-motional calculation to include the possibility of a fully anisotropic rotational diffusion tensor,  $\mathbf{R}$ . In the Appendix, we give the expressions needed to modify the slow-motional EPR line-shape calculations to accommodate the general case  $R_x \neq R_y \neq R_z$  for a Brownian model. Included are modifications needed to represent the SLE in the presence of an orienting potential. Although potential terms are not needed in the present work on isotropic solvents, we have included them with a view toward future applications in the study of dynamics in ordered phases.<sup>12</sup> (Note that non-Brownian models in the case of an ordering potential and/or a fully anisotropic  $\mathbf{R}$  would require a more general approach outlined in ref 4).

At 250 GHz, the matrices required for calculating spectra within the context of the stochastic Liouville equation (SLE) formalism are considerably larger than at X-band. For example, to fit near rigid limit spectra for the Brownian diffusion model requires a matrix of dimension 4685 with a maximum  $L$  quantum number ( $l_{\text{emx}}$ ) of 48 at 250 GHz (compared with a dimension 380 and an  $l_{\text{emx}}$  of 14 for similar motional rates of 9.5 GHz). For approximate free or jump diffusion, the required basis sets are considerably larger: jump diffusion requires a dimension of 23 234 corresponding to  $l_{\text{emx}} = 142$  for near rigid limit spectra at 250 GHz. Such calculations would be prohibitive without the advantages of the Lanczos and conjugate-gradient methods that we employ, which are described elsewhere.<sup>9</sup>

Three different models<sup>8,9</sup> for the rotational diffusion were utilized in our analysis: (1) *Brownian diffusion*, in which the molecule reorients around a given axis via infinitesimal steps with a diffusion coefficient  $R$ , (2) *moderate jump diffusion*, in which the molecule has a fixed orientation for some average residence time  $\tau$  and then “jumps” through an average angle of  $(6R\tau)^{1/2}$  radians, and (3) *approximate free diffusion*, a model intermediate to Brownian and jump diffusion in which the molecule rotates freely with a rotational rate  $R$  and then reorients instantaneously after an average time  $\tau$ .

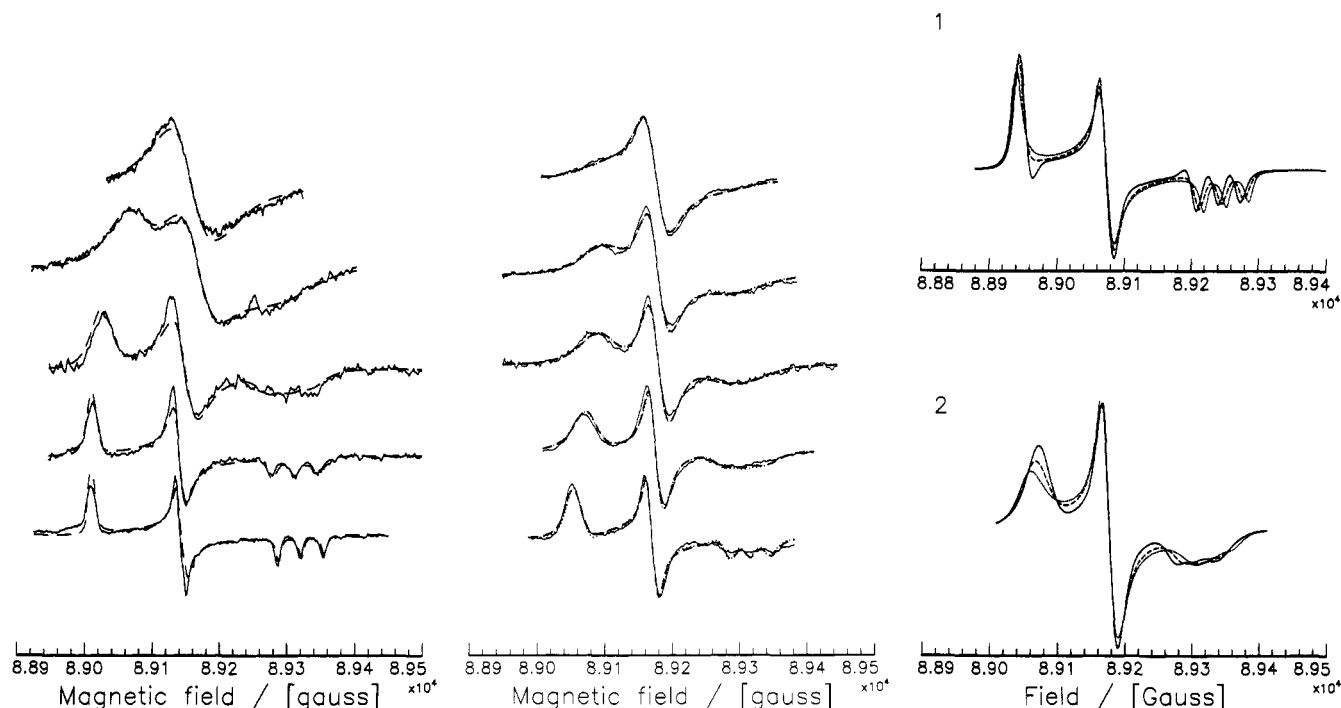


**Figure 3.** (a, left) Selected slow-motional 250-GHz EPR spectra of PDT in toluene-*d*8 (solid lines) at temperatures of (top to bottom) -97, -107, -118, -128, and -134 °C. Dashed lines show least-squares spectral fits for approximate free diffusion with  $\tau_R$  values (from top to bottom) of  $4.2 \times 10^{-10}$ ,  $1.2 \times 10^{-9}$ ,  $3.4 \times 10^{-9}$ ,  $1.5 \times 10^{-8}$ , and  $3.5 \times 10^{-7}$  s. (b, middle) Slow-motional 250-GHz EPR spectra of CSL in toluene (solid lines) at temperatures of (top to bottom) -86, -92, -97, -106, and -116 °C. Dashed lines show least-squares fits to Brownian diffusion and dotted lines those for the mixed diffusion model described in the text. From top to bottom,  $\tau_R$  values for the mixed model are  $1.6 \times 10^{-9}$ ,  $2.5 \times 10^{-9}$ ,  $5.0 \times 10^{-9}$ ,  $7.9 \times 10^{-9}$ , and  $2.5 \times 10^{-8}$  s. (c, right) Comparison of best fit spectra for the different models: (1) PDT/toluene-*d*8 at -128 °C, Brownian diffusion (—), free diffusion (---), jump diffusion (···); (2) CSL/toluene at -106 °C; Brownian diffusion (—), free diffusion (---), jump diffusion (···). The respective values of  $\tau_R$  for each model appear in Figure 4.

In order to obtain starting values for the dynamic variables used in the least-squares fitting procedure, we used the rotational anisotropy parameters  $\rho_x = 1.8 \pm 0.2$  and  $\rho_y = 1.5 \pm 0.3$  (referred to the  $x_m$ ,  $y_m$ , and  $z_m$  axes) determined from the fast-motional line widths measured at 250 and 9.5 GHz as described previously. For PDT, this analysis suggests that the motion is fastest about the magnetic  $x$  axis (along the N–O bond), and slowest about magnetic  $z$  (along the nitrogen p-orbital) but also that the deviation of the diffusion tensor from axial is small, i.e.,  $N_{xy} \equiv \rho_x/\rho_y$  is close to unity. For our slow-motional analysis, we took the magnetic axes to coincide with the diffusional axes. The fits to the experimental spectra proved to be rather insensitive to small deviations from axial anisotropy of  $\mathbf{R}$ . For example, letting  $N_{xy}$  vary over the range 0.3–3.0 produced a change in  $\chi^2$  of only about 2% for the Brownian model. For this reason, and in order to study non-Brownian models, we set  $N_{xy}$  to unity and the major (axial) diffusional anisotropy, defined as  $N = R_z/(R_x R_y)^{1/2}$ , to the value of 1.6. Only the geometric mean of the three diffusion tensor components,  $R_{\text{avg}} = (R_x R_y R_z)^{1/3}$ , was varied. The fitting procedure also included a variable parameter to account for the small amount of inhomogeneous line width present in the spectra.

For CSL, the larger anisotropy of the motion expected does influence the slow-motional spectra appreciably, so we did not initially fix the ratios of the diffusion tensor components during our analysis as was done for PDT. Instead, the results from the fast-motional analysis were used primarily as an independent check of the sensitivity and reliability of the slow-motional spectra for determining rotational anisotropy. For CSL the difference between the magnetic axes and the molecular diffusion axes was taken into account, which required the introduction of a “diffusion tilt angle”,  $\beta_d$ , as shown in the inset of Figure 1 and noted above. Varying  $\beta_d$  in the fitting procedure did not produce a significant improvement in the  $\chi^2$  of the fit; thus,  $\beta_d$  was fixed at the value  $15^\circ$  from molecular models<sup>15</sup> for all subsequent analysis of the CSL data. We also attempted to vary  $R_{\text{avg}}$ ,  $N_y \equiv R_{y_m}/(R_{x_m} R_{z_m})^{1/2}$ , and  $\rho_x \equiv R_{x_m}/R_{z_m}$ , but the spectra proved to

have a limited sensitivity to  $\rho_x$ , with the result that varying all components of the diffusion tensor simultaneously led to difficulties in convergence. In all the slow-motional fits, we fixed  $\rho_x = 1$ , which influenced the final  $\chi^2$  by less than 2% compared to using the fast-motional value of 0.5.

In order to compare results from the slow- and fast-motional analyses of CSL, it was necessary to assess the effects of the diffusion tilt angle on the latter, which were not included in the simplified AVE used to determine  $\rho_x$  and  $\rho_y$ .<sup>24</sup> The slow-motional program was used to calculate a series of motionally-narrowed spectra for different  $\rho_x$  and  $\rho_y$  values, from which a numerical approximation to  $A/B$  as a function of  $(\rho_x, \rho_y)$  was obtained. This approximation was then used to derive the  $\rho_y$  vs  $\rho_x$  curve for the experimental  $A/B$  ratio in order to compare it with the AVE. The procedure was carried out for  $\beta_d = 0^\circ$  to verify the consistency between the slow-motional programs and the AVE and for  $\beta_d = 15^\circ$  to determine the effects of the diffusion tilt. Our results for  $\beta_d = 0^\circ$  agreed very well with the AVE.<sup>24</sup> The  $A/B$  ratio for  $\beta_d = 15^\circ$  did not deviate from that calculated for  $\beta_d = 0^\circ$  by more than 1% in the region of interest  $(\rho_x, \rho_y) = (0.5, 3.0)$ . This is less than half of the experimental uncertainty in  $A/B$ . For this reason, we neglected diffusion tilt in subsequent comparisons of our fast-motional and slow-motional analyses of CSL.

A physical quantity of interest in our analysis is the rotational correlation time  $\tau_R$  as a function of  $\eta/T$ . This may be defined in terms of a mean diffusional rate,  $R_{\text{avg}}$ , and the “model-dependent” parameter  $B_2^{(l)}$ .<sup>8,25</sup>

$$\tau_R = \frac{1}{6B_2^{(l)}R_{\text{avg}}} \quad (1)$$

where the canonical models (for which  $R_{\text{avg}}\tau = 1$ ) yield

$$B_L^{(l)} = \frac{1}{(1 + L(L + 1))^l} \quad (2)$$

The exponent  $l$  in this equation is 0, 1/2, and 1 for Brownian,

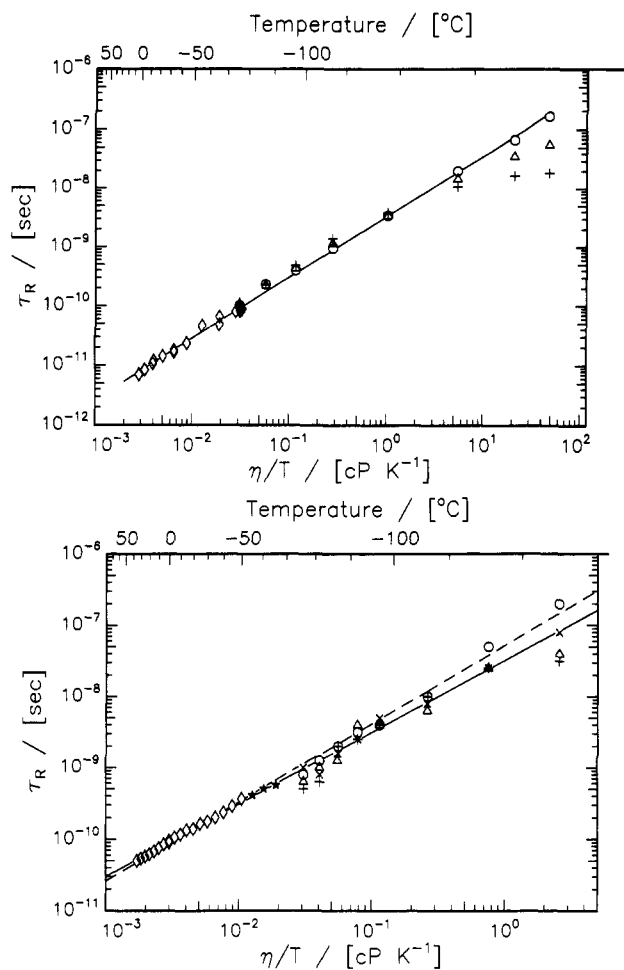


**Figure 4.** Plots of  $\tau_R$  obtained from least-squares fits of slow-motional 250-GHz EPR spectra for two spin probes using different diffusional models as a function of  $\eta/T$ . (a, upper) PDT in toluene- $d_8$ :  $\tau_R$  derived from (O) Brownian diffusion, ( $\Delta$ ) approximate free diffusion, (+) jump diffusion, and ( $\diamond$ ) fast-motional  $B_{250}$  line width parameter. Solid line is a fit to  $\tau_R$  derived from the combined Brownian and fast-motional data. (b, lower) CSL in toluene:  $\tau_R$  derived from (O) Brownian diffusion, ( $\Delta$ ) approximate free diffusion, (+) jump diffusion, ( $\times$ ) the mixed diffusion model described in the text, ( $\diamond$ ) fast-motional  $B_{250}$  line width parameter, and ( $\star$ ) least-squares fitting in the model-independent incipient slow-motional region. Lines represent fits to  $\tau_R$  derived from the combined model-independent and mixed diffusion (solid line) or Brownian diffusion (dashed line) data.

free, and jump diffusion, so that  $B_2^{(0)}$  assumes values of 1,  $(7)^{-1/2}$ , and  $(7)^{-1}$  for each of these models, respectively. This definition for  $\tau_R$  assures that in the motional-narrowing limit all three diffusional models will yield the same line width for a given  $R_{\text{avg}}^{1,8,25}$ .

Figure 4 parts a and b show plots of  $\tau_R$  vs  $\eta/T$  determined using each of the three diffusional models studied for both PDT (Figure 4a) and CSL (Figure 4b). For the higher temperatures within the slow-motional regime, as well as the fast-motional regime, all three models give quite similar  $\tau_R$  values. However, toward the rigid limit, the best-fit  $\tau_R$  values obtained from the different models begin to diverge significantly as a function of temperature. From the plots of  $\tau_R$  vs  $\eta/T$ , it is clear that the Brownian model falls closest to a straight line (i.e., Stokes-Einstein behavior) in the case of PDT and also CSL.

A more direct criterion for assessing the suitability of a given diffusional model is the estimated  $\chi^2$  returned by the least-squares procedure, which may be compared for the different models in order to determine objectively which one best fits the data. Figure 5 parts a and b shows  $\chi^2$  plotted vs  $\eta/T$  for each of the models studied; these results indicate that the best fit to the spectra is given by approximate free diffusion for the PDT spin probe, and

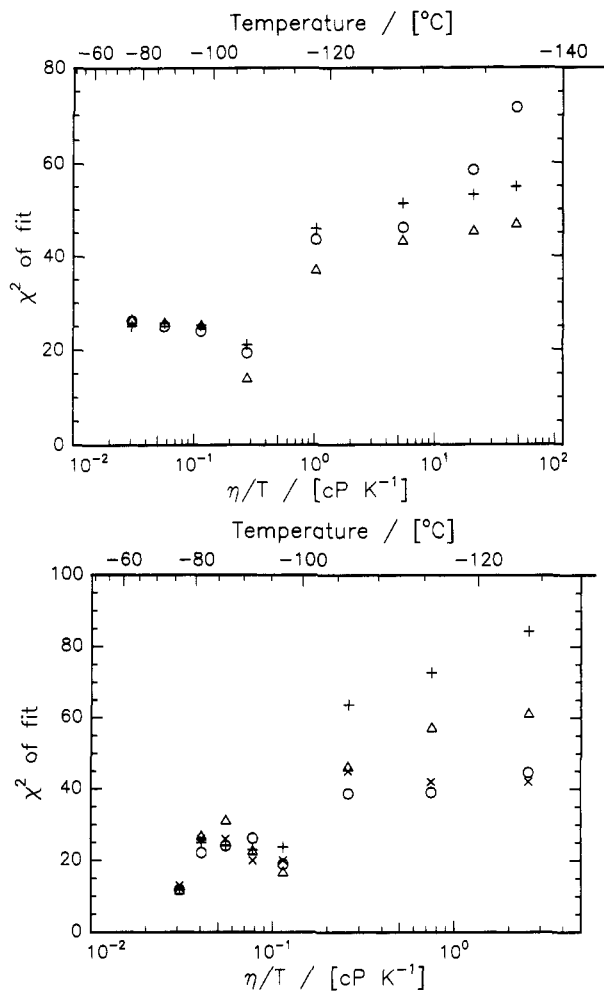


**Figure 5.**  $\chi^2$  for fits of slow-motional 250-GHz EPR spectra for two spin probes using different diffusional models. (a, upper) PDT in toluene- $d_8$ : (O) Brownian diffusion, ( $\Delta$ ) approximate free diffusion, (+) jump diffusion. (b, lower) CSL in toluene: (O) Brownian diffusion; ( $\Delta$ ) approximate free diffusion, (+) jump diffusion, and ( $\times$ ) mixed diffusion. Results are plotted vs  $\eta/T$  to facilitate comparison with Figure 4.

Brownian diffusion for CSL. We will comment on the apparent discrepancy between the  $\chi^2$  and the  $\tau_R$  vs  $\eta/T$  results for PDT in toluene- $d_8$  in the discussion below.

The best calculated fits obtained for each of the experimental spectra, using approximate free diffusion for PDT and Brownian diffusion for CSL, are shown together with the experimental data by the dashed lines in Figure 3 parts a and b. In Figure 3c, we compare the best fits of the different models in the model-sensitive region for PDT and CSL.

## Discussion

**Sensitivity of 250-GHz Slow-Motional Spectra to Diffusional Model.** The major advantage of high-field EPR for studying the rotational diffusion of spin probes derives primarily from the fact that the spectral regions corresponding to different orientations of the probe are well separated from one another, as we have noted in the Introduction. In contrast, at conventional EPR frequencies, spectral regions corresponding to the  $x$ ,  $y$ , and  $z$  orientations are not well resolved for nitroxides. This is because the contributions of the hyperfine and  $g$  tensors to the anisotropic part of the spin Hamiltonian are comparable at conventional EPR frequencies, whereas at 250 GHz, the  $g$  tensor dominates and provides the orientational resolution. Ideally, in the slow-motional regime one should study how the homogeneous line widths vary across the spectrum. The orientation dependence of these widths (and relaxation rates in general) have been shown to be very sensitive indicators of the nature of the motion both

in terms of the precise model of rotational reorientation as well as the degree of anisotropy.<sup>26,27</sup>

Slow-motional spectra obtained at 250 GHz exhibit different degrees of sensitivity to the diffusional model throughout the slow-motional regime. For faster motions, near the limit of motional narrowing, one finds that the spectra are rather insensitive to the type of diffusional model used. However, spectral differences between different types of diffusional models become distinguishable in the middle of the slow-motional regime. Very near the rigid limit, the spectrum approaches the rigid "powder pattern" line shape and must become model-independent. It is interesting that for 250 GHz this model sensitivity increases until one is quite near the rigid limit, thereby supplying a larger model-sensitive region than one has at 9 GHz.

Qualitatively, the major changes in the spectral line shape as the motional rates increase from the rigid limit are (i) an increase in the homogeneous line widths due to motion, (ii) a shift of the positions of the "turning points" of the spectrum at  $g_x$ ,  $g_y$ , and  $g_z$  toward the average  $g$  value of the spectrum as the motion starts to average the spectrum, and (iii) a "filling-in" of intensity in the spectral regions between the turning points. Different diffusional models produce these effects to different degrees: for example, Brownian diffusion affects the positions of the turning points most strongly at the onset of motion, whereas jump diffusion mainly affects the line widths at the same motional rates. These observations are consistent with the qualitative conclusions of Lebedev and co-workers<sup>11,10</sup> concerning the  $z$  region of the spectrum, but we extend them to the entire spectrum. The  $y$  region, which is typically close to  $\langle g \rangle = (g_x + g_y + g_z)/3$  for nitroxides, does not shift significantly but does exhibit  $R$ -dependent broadening for the systems studied in this work.

More specifically, at 250 GHz, the three canonical diffusion models have the following qualitative behavior upon going from the rigid limit into the model-sensitive region. For jump diffusion, the  $g_x$  and  $g_z$  peaks broaden but do not shift appreciably until well into the slow-motional regime, and they exhibit significant spectral intensity between the canonical orientations. In the case of free diffusion, the  $g_x$  and  $g_z$  peaks do not separate or narrow as rapidly as in the case of jump diffusion. Moreover, the spectral intensity between the canonical orientations is less than what a jump model would predict. Finally, for Brownian diffusion, the  $g_x$  and  $g_z$  regions shift rapidly with increasing motion but broaden slowly relative to the other models. The spectral intensity (in first-derivative representation) remains close to the base line between the extremes of the spectrum and actually dips below the base line on the high-field side of the  $g_x$  region while rising above the base line on the low-field side of the  $g_z$  peaks, over a significant range of rotational correlation times.

The differences just described can be observed in the temperature dependences of the 250-GHz slow-motional line shapes of PDT and CSL shown in Figure 3 parts a–c. In the case of CSL, the peaks at the extremes of the spectrum shift readily as the temperature is increased from the rigid limit and only broaden substantially at higher temperatures. In contrast, the extrema of the PDT spectra broaden significantly before any appreciable shift in the peak positions occurs. Thus, a simple inspection of the spectra indicates that the motion of PDT is best described by a jump or free diffusion model, while the CSL spectra appear to exhibit the features of Brownian diffusion. These qualitative observations are consistent with the more quantitative results shown in Figures 4 and 5 and discussed below. Although quantitative line-shape analysis provides a more definitive indication of the diffusional model, it is worth noting that the high spectral resolution at 250 GHz does allow one to make a good initial estimate of the motional model much more easily than at 9 GHz.

For a more complete understanding of the line-shape behavior, a full calculation using the SLE is necessary. The positions and

shapes of the features across the entire spectrum may be studied as a function of temperature, providing sensitive indicators of the motional model. Furthermore, the use of nonlinear least-squares analysis gives an objective estimate of uncertainties in the model parameters as well as correlations amongst them.

An alternative approach has been developed by Lebedev and co-workers<sup>11</sup> for spectra obtained at 140 GHz. It concentrates on the positions and widths of the three resolved peaks in the  $g_z$  region of nitroxide spectra, on the assumption that pseudosecular contributions (i.e., those terms in the spin Hamiltonian that depend upon the  $S_z I_{\pm}$  operator) to the line shape may be neglected for this region of the spectrum. Such an assumption greatly reduces the computational effort required for the simulations. For example, removing the contributions due to pseudosecular terms reduced the stochastic Liouville matrix dimension by a factor of approximately 9 for each of the three allowed electron spin transitions in a <sup>14</sup>N nitroxide ( $I = 1$ ). In order to decide whether this approach might be useful for the systems studied at 250 GHz, we compared a full spectral simulation with one that did not include pseudosecular contributions. We found that the simplified calculation did display numerous differences from the full calculation. Even in the  $g_z$  region of the spectrum the intensities for the  $z$  peaks were not correctly predicted. For these reasons, we used full calculations for all the spectra analyzed in this work. The simplified analysis of Lebedev was also limited to the two extreme cases of strong jump and Brownian diffusion. Furthermore, since it is restricted to the  $z$  canonical orientation, it cannot treat cases in which there is different diffusional behavior for different molecular axes (cf. discussion below).

**Slow Motion of the PDT Spin Probe.** As discussed above, the rotational anisotropy of PDT as determined by combined fast-motional line-width analysis at 250 and 9.5 GHz is rather small, consistent with what one might expect given the nearly spherical shape of the molecule. PDT thus provides a demanding test of the sensitivity to rotational anisotropy of high-field EPR in the slow-motional regime. We find that in general slow-motional spectra are less sensitive to the small anisotropies in the rotational diffusion tensor exhibited by PDT than fast-motional studies at high field. In the model-sensitive region, allowing  $N$  and  $N_{xy}$  to vary did improve the fits somewhat, but not by a statistically significant amount. However, as we have seen, the slow-motional spectra of PDT in toluene- $d_8$  do reveal significant deviations from Brownian diffusion, and correspond most closely to the model of approximate free diffusion. This is consistent with previous slow-motional CW-EPR results at 9.5 GHz.<sup>2</sup> However, the graph of  $\tau_R$  vs  $\eta/T$  in Figure 4a shows a linear dependence for a Brownian model but not for free diffusion. One must be cautious in using this observation, because (i) it involves extrapolation of the data of Barlow *et al.*<sup>16</sup> into the supercooled region of toluene for 2 orders of magnitude greater  $\eta/T$  values than they actually measured and (ii) there is no guarantee that a simple linear dependence of  $\tau_R$  upon  $\eta/T$  will actually be maintained over nearly 5 orders of magnitude.<sup>3</sup> Of course, the apparent discrepancy between this  $\tau_R$  vs  $\eta/T$  fit to a linear relation for Brownian motion and the detailed spectral fits, which definitely favor free diffusion, could be suggestive that a better model of rotational reorientation is required. Previously, it was pointed out that a model based upon fluctuating torques might resolve a similar discrepancy between two-dimensional electron spin-echo results (which favored Brownian motion) and CW results (which favored a jump diffusion model, although the predictions of a moderate jump or free diffusion model were indistinguishable at 9.5 GHz) for PDT in 85% glycerol/15% water.<sup>26,27</sup> The fluctuating torques model is based on the notion that the PDT is comparable in size to the solvent toluene molecules so that collective relaxation of solute and solvent molecules may be required.<sup>2</sup> Recently, this and related collective models of rotational motions in liquids have been analyzed in great detail.<sup>28</sup> It would be of interest to

incorporate such "enhanced" models into the slow-motional EPR theory to compare with the 250-GHz EPR spectra, although this is likely to be a significant computational challenge.

**Slow Motion of the CSL Spin Probe.** In contrast to PDT, high-field slow-motional CSL spectra are reasonably sensitive to the main (axial) motional anisotropy of the molecule,  $N$ , because the anisotropy of the motion is significantly larger than that of PDT. However, as was the case for PDT, they are not sensitive to small deviations from axial anisotropy.

The data for CSL show that the rotational diffusion for this probe is best described by a Brownian diffusion model. This conclusion is on the whole consistent with what one would intuitively expect for this probe, given its large size relative to that of the solvent molecules. Thus, the high-field results provide reasonable experimental evidence for the Brownian model that has been widely assumed for CSL in model membrane studies.<sup>6,21,22</sup>

Interestingly, the  $N$  value obtained for CSL from the slow-motional data depends significantly on the diffusional model used. The values of  $N$  that we obtain for CSL for the various models are as follows:  $N_{\text{Brownian}} = 9.4 \pm 0.2$ ,  $N_{\text{free}} = 3.5 \pm 1$ ,  $N_{\text{jump}} = 4.3 \pm 0.8$ . The values for jump and free diffusion are closer to the fast-motional value (which we can take as  $N_y \equiv R_{y_m}/(R_{x_m}R_{z_m})^{1/2} = 4.3$ ; cf. Results) and also more consistent with simple geometric considerations (cf. below). On the other hand, Brownian diffusion gives a significantly better overall fit to the experimental spectra, particularly at lower temperatures, and the uncertainty in  $N_{\text{Brownian}}$  is much lower than that in  $N_{\text{free}}$  or  $N_{\text{jump}}$ . These considerations suggest that overall Brownian diffusion is the most appropriate model of the three to describe CSL despite the large  $N$  value found for this model.

The question thus remains why the value of  $N$  determined from the slow-motional analysis using Brownian diffusion differs so significantly from that obtained by the fast-motional analysis. Given that the CSL probe is cigar-shaped, it is conceivable that the details of the rotational diffusion depend upon the axis about which the diffusion occurs, even though the diffusion of the "major" axis is probably Brownian.

In order to test this hypothesis, we constructed a "mixed" model of diffusion, which allowed Brownian diffusion about the short axes of the molecule ( $R_{\perp}$ ) and approximate free diffusion about the long axis ( $R_{\parallel}$ ). The matrix elements of the diffusion operator in this model are (for  $R_{\parallel}\tau = 1$ ):<sup>9</sup>

$$\langle L_1 K_1 M_1 \dots | \vec{I}_{\text{iso}} | L_2 K_2 M_2 \dots \rangle = R_{\perp} L_1 (L_1 + 1) + \frac{(R_{\parallel} - R_{\perp}) K_1^2}{(1 + K_1^2)^{1/2}} \quad (3)$$

If one defines as  $N_{\text{eff}} = R_{\parallel}^{\text{eff}}/R_{\perp}$ , where  $R_{\parallel}^{\text{eff}} = 5^{1/2}(R_{\parallel} - R_{\perp})$  from eq 3 by analogy to eq 1,<sup>5,9</sup> then one finds from the least-squares  $R_{\parallel}$  and  $R_{\perp}$  that  $N_{\text{eff}} = 4.5 \pm 0.3$  over the entire slow-motional range. The best fits for this model are shown in Figure 3b. Also, the  $\tau_{\text{R}}$ , defined as  $\tau_{\text{R}} = [6R_{\perp}(N_{\text{eff}})^{1/2}]^{-1}$  for the mixed model, is found to be linear in  $\eta/T$  as shown in Figure 4b. (Here, for  $\tau_{\text{R}} \propto (\eta/T)^{\alpha}$  one obtains  $\alpha = 1.01 \pm 0.01$  for the mixed model and  $\alpha = 1.09 \pm 0.01$  for the Brownian model.) The  $\chi^2$  for this mixed model is comparable to that from the Brownian models. Thus, while the  $\chi^2$  from the spectral fit does not by itself justify a mixed diffusional model for CSL, the  $N$  value predicted by such a model is very close to that determined from the fast-motional analysis ( $N = 4.3 \pm 0.2$ ). The use of a mixed diffusional model for PDT might succeed in reconciling the above result that for PDT free diffusion gives the best fits but Brownian diffusion gives the best  $\eta/T$  dependence of  $\tau_{\text{R}}$ . This remains to be studied.

We now review briefly the hydrodynamic model to calculate  $N$ . Further details may be found in the treatise of Lamb.<sup>29</sup> In general, one may determine the components of the diffusion

tensor from the friction tensor  $\beta$  as follows:

$$R_{\parallel} = kT/\beta_{\parallel} \quad (4)$$

The spin probe CSL is approximately cylindrical with a length 24 Å and diameter 6 Å.<sup>30</sup> We will therefore take the radii of the equivalent ellipsoid to be  $a_1 = 12$  Å and  $a_2 = 3$  Å. In the limit of axial diffusion for a prolate ellipsoid,  $N$  is given by the following formula:

$$N = \frac{R_{\parallel}}{R_{\perp}} = \left(1 + \frac{a_1^2}{a_2^2}\right) \frac{2 - (a_2^2/a_1)S}{(2 - (a_2/a_1)^2)a_1S - 2} \quad (5)$$

where

$$S = \frac{2}{(a_1^2 - a_2^2)^{1/2}} \ln \left( \frac{a_1 + (a_1^2 - a_2^2)^{1/2}}{a_2} \right) \quad (6)$$

One finds  $N = 4.7$  for the parameters given above. This is to be compared with the fast-motional analysis which yields  $N \approx 4.3$  (or our slow-motional fit of  $N \approx 4.5$  for the "mixed" diffusional model). The equivalent ellipsoid may also be used to compute an effective hydrodynamic radius as discussed in ref 20. For axial diffusion, one finds

$$r_e^3 = \left(\frac{4N}{3}\right)^{1/2} \frac{1}{Q_2} \quad (7)$$

where

$$Q_2 = \frac{a_1}{(a_1^2 - a_2^2)a_2^2} + \frac{1}{(a_1^2 - a_2^2)^{3/2}} \ln \left( \frac{a_1 - (a_1^2 - a_2^2)^{1/2}}{a_1 + (a_1^2 - a_2^2)^{1/2}} \right) \quad (8)$$

Using that definition,  $r_e = 7.01$  Å. The equivalent hydrodynamic radius may be compared with the observed hydrodynamic radius via the Stokes-Einstein relation

$$\tau_{\text{R}} = \frac{4}{3} \pi r_e^3 \frac{\eta}{kT} \quad (9)$$

The slope of  $\tau_{\text{R}}$  vs  $\eta/kT$  gives  $r_e^{\text{obs}}$ . PDT in toluene- $d_8$  has been analyzed in this way previously.<sup>2,20</sup> CSL in toluene (this work) yields  $r_e^{\text{obs}} = 5.6$  Å. The difference between the hydrodynamic effective radius and the observed effective radius may be attributed to a slip factor  $\kappa = (r_e^{\text{obs}}/r_e)^3 = 0.5$  for CSL in toluene. (One may, of course, have an asymmetry in the slip factor as well).

## Conclusions

The 250-GHz EPR line shapes of two spin probes, PDT and CSL, have been studied in isotropic solvents throughout the slow-motional regime. The slow-motional spectra at this high frequency are significantly more sensitive to the microscopic diffusional model than at conventional EPR frequencies and allow one to distinguish between Brownian diffusion and different non-Brownian effects, but this does require full spectral simulations based on the stochastic Liouville equation. PDT in toluene- $d_8$  is best fit by an approximate free diffusion model, consistent with previous CW-EPR results obtained at 9.5 GHz.<sup>2</sup> The temperature dependence of  $\tau_{\text{R}}$  vs  $\eta/T$  indicates a preference for Brownian diffusion, however. CSL in toluene is best fit either with a model of overall Brownian diffusion or a mixed one in which the motion of the long axis is Brownian, whereas motion around this axis is free diffusional. The value of the motional anisotropy obtained with the mixed model is in good agreement with that determined from fast-motional line widths, as well as from what may be expected from geometric considerations of the CSL molecule, but the Brownian model leads to a larger anisotropy. While slow-motional spectra at 250 GHz are reasonably sensitive to rotational anisotropy, they appear to be somewhat less sensitive than fast-motional line widths at this frequency.

**Acknowledgment.** We are grateful to Mr. David Hanauer for assistance with the 9.5-GHz spectra, Ms. Diane Crepeau for



programming the graphical interface of program NLSL, and Dr. David Schneider for useful discussions. This work was supported by NIH grants GM25862 and RR07126 and NSF Grant CHE 9312167. D.E.B. is a NIH NRSA GM-12924 recipient. Computations were performed at the Cornell National Supercomputer Facility.

### Appendix

In this Appendix we give the additional theoretical expressions needed to extend existing slow-motional EPR theory<sup>5</sup> to include the general case of a completely anisotropic rotational diffusion tensor, i.e.,  $\mathbf{R} = \text{diag}\{R_x, R_y, R_z\}$  where  $R_x \neq R_y \neq R_z$ . The expressions given below refer extensively to those derived in Appendix A of ref 5.

We consider first the isotropic diffusion operator,  $\Gamma_{\text{iso}} = \mathbf{J} \cdot \mathbf{R} \cdot \mathbf{J}$ , where  $\mathbf{J}$  is the generator of infinitesimal rotations for a rotating body. In terms of raising and lowering operators,  $\mathbf{J} \cdot \mathbf{R} \cdot \mathbf{J}$  may be written as

$$\begin{aligned} \mathbf{J} \cdot \mathbf{R} \cdot \mathbf{J} &= J_x^2 R_x + J_y^2 R_y + J_z^2 R_z \\ &= \frac{R_x}{4}(J_+ + J_-)^2 - \frac{R_y}{4}(J_+ - J_-)^2 + J_z^2 R_z \\ &= \frac{R_x - R_y}{4}(J_+^2 + J_-^2) + \frac{R_x + R_y}{4}(J_+ J_- + J_- J_+) + J_z^2 R_z \end{aligned} \quad (\text{A1})$$

To obtain the matrix elements of  $\mathbf{J} \cdot \mathbf{R} \cdot \mathbf{J}$  in the basis set of generalized spherical harmonics,  $D_{M,K}^L(\Omega)$ , we first write down the effect of each  $\mathbf{J}$  tensor component operating on a  $D_{M,K}^L(\Omega)$ :

$$\begin{aligned} J_{\pm} D_{M,K}^L(\Omega) &= M_{\pm}(L,K) D_{M,K \pm 1}^L(\Omega) \\ (J_{\pm})^2 D_{M,K}^L(\Omega) &= N_{\pm}(L,K) D_{M,K \pm 2}^L(\Omega) \\ J_{\pm} J_{\mp} D_{M,K}^L(\Omega) &= M_{\mp}(L,K) D_{M,K}^L(\Omega) \end{aligned} \quad (\text{A2})$$

where  $M_{\pm}(L,K) \equiv [(L \mp K)(L \pm K + 1)]^{1/2}$  and  $N_{\pm}(L,K) \equiv [(L \mp K - 1)(L \mp K)(L \pm K + 1)(L \pm K + 2)]^{1/2}$ . Using these expressions, the matrix elements of  $\Gamma_{\text{iso}}$  may be written

$$\begin{aligned} \langle L_1 K_1 M_1 | \Gamma_{\text{iso}} | L_2 K_2 M_2 \rangle &= \\ \delta_{L_1, L_2} \delta_{M_1, M_2} \left\{ \delta_{K_1, K_2} \left[ \frac{R_x + R_y}{2} (L_1(L_1 + 1) - K_1^2) + R_z K_1^2 \right] + \right. \\ \left. \frac{R_x - R_y}{4} [\delta_{K_1 - 2, K_2} N_+(L_1, K_1 - 2) + \delta_{K_1 + 2, K_2} N_-(L_1, K_1 + 2)] \right\} \end{aligned} \quad (\text{A3})$$

In the presence of an orienting potential  $U(\Omega)$  in anisotropic liquids, the symmetrized potential-dependent part of the diffusion operator,  $\tilde{\Gamma}_U$ , must also be modified. In operator form, the diffusion operator  $\tilde{\Gamma}$  in the presence of a potential is given by

$$\begin{aligned} \tilde{\Gamma} &= \left( J - \frac{JU}{2kT} \right) R \left( J + \frac{JU}{2kT} \right) \\ &= J \cdot \mathbf{R} \cdot J - \frac{1}{2kT} (JU) \cdot \mathbf{R} \cdot J + \frac{1}{2kT} J \cdot \mathbf{R} \cdot (JU) - \\ &\quad \frac{1}{4k^2 T^2} (JU) \cdot \mathbf{R} \cdot (JU) \\ &= \tilde{\Gamma}_{\text{iso}} + \frac{1}{2kT} (J \cdot \mathbf{R} \cdot J) U = \frac{1}{4k^2 T^2} (JU) \cdot \mathbf{R} \cdot (JU) \\ &= \tilde{\Gamma}_{\text{iso}} + \tilde{\Gamma}_U \end{aligned} \quad (\text{A4})$$

This potential is expressed in the usual way as an expansion in terms of spherical harmonics:

$$U(\Omega) = -kT \sum_{L,K} \lambda_K^L D_{0,K}^L(\Omega) \quad (\text{A5})$$

where the prime indicates that the summation is restricted to even values of  $L$  and  $K$  up to 4, and the expansion coefficients

have the property that  $\lambda_K^L = \lambda_{-K}^L = \lambda_K^{L*}$ . Using the definition for the potential given in eq A5 and the properties of the raising and lowering operators given in eqs A2, the expression for  $\tilde{\Gamma}_U$  may be recast in the form

$$\tilde{\Gamma}_U = \sum_{L=0}^{2L_{\text{ptmx}}} \sum_{K=0}^{K_{\text{ptmx}}} \lambda_K^L D_{0,K}^L(\Omega) \quad (\text{A6})$$

where  $L_{\text{ptmx}}$  and  $K_{\text{ptmx}}$  specify the maximum  $L$  and  $K$  indices used in the expansion of the potential and  $LK_{\text{ptmx}}$  is the lesser of  $L_{\text{ptmx}}$  and  $2K_{\text{ptmx}} + 2$ . For fully anisotropic diffusion, the coefficients  $\lambda_K^L$  are given by

$$\begin{aligned} \lambda_K^L &= \\ \frac{1}{2} &\left[ (\lambda_{K+2}^L N_-(L, K+2) + \lambda_{K-2}^L N_+(L, K-2)) \frac{R_x - R_y}{4} + \right. \\ &\quad \left. \lambda_K^L (L(L+1) - K^2) \frac{R_x + R_y}{2} + \lambda_K^L K^2 R_z \right] - \\ &\quad \frac{(2L+1)}{4} \sum_{L_1, K_1, L_2, K_2} \lambda_{K_1}^{L_1} \lambda_{K_2}^{L_2} \begin{pmatrix} L_1 & L & L_2 \\ 0 & 0 & 0 \end{pmatrix} \times \\ &\quad \left\{ \frac{R_x - R_y}{4} \left[ M_+(L_1, K_1) M_+(L_2, K_2) \begin{pmatrix} L_1 & L & L_2 \\ K_1 + 1 & -K & K_2 + 1 \end{pmatrix} + \right. \right. \\ &\quad \left. \left. M_-(L_1, K_1) M_-(L_2, K_2) \begin{pmatrix} L_1 & L & L_2 \\ K_1 - 1 & -K & K_2 - 1 \end{pmatrix} \right] + \right. \\ &\quad \left. \frac{R_x + R_y}{2} M_+(L_1, K_1) M_-(L_2, K_2) \begin{pmatrix} L_1 & L & L_2 \\ K_1 + 1 & -K & K_2 - 1 \end{pmatrix} + \right. \\ &\quad \left. R_z K_1 K_2 \begin{pmatrix} L_1 & L & L_2 \\ K_1 & -K & K_2 \end{pmatrix} \right\} \end{aligned} \quad (\text{A7})$$

which leads to the following expression for the matrix elements of  $\tilde{\Gamma}_U$ :

$$\begin{aligned} \langle L_1 M_1 K_1 | \tilde{\Gamma}_U | L_2 M_2 K_2 \rangle &= \\ \delta_{M_1, M_2} \sum_{L'} \lambda_{K_1 - K_2}^{L'} N(L_1, L_2) (-1)^{K_1 + M_1} \times \\ &\quad \begin{pmatrix} L_1 & L & L_2 \\ M_1 & 0 & M_2 \end{pmatrix} \begin{pmatrix} L_1 & L & L_2 \\ K_1 & K_2 - K_1 & K_2 \end{pmatrix} \end{aligned} \quad (\text{A8})$$

where  $N(L_1, L_2) = (2L_1 + 1)^{1/2} (2L_2 + 1)^{1/2}$  and we have made use of the identity<sup>31</sup>

$$\begin{aligned} D_{M_1, M_1}^{J_1}(\Omega) D_{M_2, M_2}^{J_2}(\Omega) &= \\ \sum_{J_3} (2J_3 + 1) &\begin{pmatrix} J_1 & J_2 & J_3 \\ M_1 & M_2 & M_3 \end{pmatrix} \times \\ &\begin{pmatrix} J_1 & J_2 & J_3 \\ M_1 & M_2 & M_3 \end{pmatrix} D_{M_3, M_3}^{J_3}(\Omega) \end{aligned} \quad (\text{A9})$$

Equation A8 differs from the expression given by Meirovitch *et al.* for the axial case (their eq A24) only in the definition of  $\lambda_{K_1 - K_2}^{L'}$  and in the range of summation. Equations A3 and A7 above reduce to eqs A15 and A23 of Meirovitch *et al.*, respectively, in the limit of axial diffusion ( $R_x = R_y$ ), as required. We also note that similar expressions for  $\tilde{\Gamma}_U$  in the case of a fully anisotropic  $\mathbf{R}$  tensor have been given by Bulthuis and Plomp<sup>32</sup> for the special case of potential coefficients with  $L \leq 2$ . Equations A7 and A8 reduce to eqs 13 of ref 32 when we substitute  $c_0^2 = 2\lambda/3$  and  $c_2^2 = (2/3)^{1/2} \rho$  and limit  $L_{\text{ptmx}}$  to 2.

To convert the stochastic Liouville matrix to the complex-



symmetric form required for the numerical methods we use, we transform the diffusion operator into the "K-symmetrized" basis defined as follows:

$$|LMKj^K \dots\rangle = [2(1 + \delta_{K',0})] \exp\left[\frac{\pi}{4}(1 - j^K)\right] \left\{ |LMK' \dots\rangle + j^K (-1)^{L+K} |LM-K' \dots\rangle \right\} \quad (\text{A10})$$

where  $K'$  is non-negative and  $j^K = \pm 1$  for  $K \neq 0$  and  $j^K = (-1)^L$  for  $K = 0$ . In this basis,  $\tilde{\Gamma}_{\text{iso}}$  is given by

$$\begin{aligned} \langle L_1 K_1 M_1 j_1^K \dots | \tilde{\Gamma}_{\text{iso}} | L_2 K_2 M_2 j_2^K \dots \rangle = \\ \delta_{L_1, L_2} \delta_{M_1, M_2} \delta_{j_1^K, j_2^K} \left\{ \delta_{K_1, K_2} \left[ \frac{R_x + R_y}{2} (L_1(L_1 + 1) - K_1^2) + \right. \right. \\ \left. \left. R_z K_1^2 \right] + (\delta_{K_1 - 2, K_2} N_+(L_1, K_1 - 2) + \delta_{K_1 + 2, K_2} N_-(L_1, K_1 + \right. \\ \left. 2)) N_K(K_1, K_2)^{-1} \left[ \frac{R_x - R_y}{4} \right] \right\} \quad (\text{A11}) \end{aligned}$$

The symmetrized potential-dependent operator,  $\tilde{\Gamma}_U$ , is given by

$$\begin{aligned} \langle L_1 K_1 M_1 j_1^K | \tilde{\Gamma}_U | L_2 K_2 M_2 j_2^K \rangle = \delta_{M_1, M_2} \delta_{j_1^K, j_2^K} N(L_1, L_2) \times \\ N_K(K_1, K_2) (-1)^{M_1 + K_1} \sum_L \begin{pmatrix} L_1 & L & L_2 \\ M_1 & 0 & -M_1 \end{pmatrix} \times \\ \left\{ X_{K_1 - K_2}^L \begin{pmatrix} L_1 & L & L_2 \\ K_1 & K_2 - K_1 & -K_2 \end{pmatrix} + \right. \\ \left. j_2^K (-1)^{L_2 + K_2} X_{K_1 + K_2}^L \begin{pmatrix} L_1 & L & L_2 \\ K_1 & -K_1 - K_2 & K_2 \end{pmatrix} \right\} \quad (\text{A12}) \end{aligned}$$

This expression reduces to that given in eq A40 of Meirovitch *et al.*<sup>5</sup> in the axial limit.

The expressions given here for fully anisotropic rotation are valid in the case of Brownian diffusion. Expressions for  $\tilde{\Gamma}$  in the case of non-Brownian diffusion are available only in the limit of an axial diffusion tensor and the absence of any orienting potential but can be extended to the more general cases by methods outlined elsewhere.<sup>4</sup>

## References and Notes

- (1) (a) Goldman, S. A.; Bruno, G. V.; Polnaszek, C. F.; Freed, J. H. *J. Chem. Phys.* **1972**, *56*, 716. (b) Goldman, S. A.; Bruno, G. V.; Freed, J. H. **1973**, *59*, 3071.
- (2) Hwang, J. S.; Mason, R. P.; Hwang, L.-P.; Freed, J. H. *J. Phys. Chem.* **1975**, *79*, 489.

- (3) Zager, S. A.; Freed, J. H. *J. Chem. Phys.* **1982**, *77*, 3344, 3360.
- (4) Polnaszek, C. F.; Freed, J. H. *J. Phys. Chem.* **1975**, *79*, 2283.
- (5) Meirovitch, E.; Ignér, D.; Ignér, E.; Moro, G.; Freed, J. H. *J. Chem. Phys.* **1982**, *77*, 3915.
- (6) Tanaka, H.; Freed, J. H. *J. Phys. Chem.* **1985**, *89*, 350.
- (7) Berliner, L. J.; Reuben, J. *Biological Magnetic Resonance, Vol. 8: Spin Labeling Theory and Applications*; Academic Press: New York, 1989.
- (8) Freed, J. H. In *Spin Labeling: Theory and Applications*; Berliner, L., Ed.; Academic Press: New York, 1976; p 53.
- (9) Schneider, D. J.; Freed, J. H. *Biological Magnetic Resonance*; Berliner, L. J., Reuben, J., Eds.; Plenum: New York, 1989; Vol. 8, p 1.
- (10) Lebedev, Ya. S. In *Modern Pulsed and Continuous Wave Electron Spin Resonance*; Kevan, L., Bowman, M. K., Eds.; Wiley: New York, 1990.
- (11) Lyubashevskaya, E. V.; Antsiferova, L. I.; Lebedev, Ya. S. *Teor. Eksp. Khim.* **1987**, *23*, 46.
- (12) Budil, D. E.; Earle, K. A.; Lynch, W. B.; Freed, J. H. *Advanced EPR: Applications in Biology and Biochemistry*; Hoff, A. J., Ed.; Elsevier: Amsterdam, 1989; Chapter 8.
- (13) Budil, D. E.; Freed, J. H. program NLSL, to be published.
- (14) Lynch, W. B.; Earle, K. A.; Freed, J. H. *Rev. Sci. Instrum.* **1988**, *59*, 1345.
- (15) Meirovitch, E.; Freed, J. H. *J. Phys. Chem.* **1984**, *88*, 4995.
- (16) Barlow, A. J.; Lamb, J.; Matheson, A. J. *Proc. R. Soc. London, A* **1966**, *292*, 322.
- (17) Zager, S. A. Ph.D. Dissertation, Cornell University, 1982.
- (18) Bales, B. In *Biological Magnetic Resonance*; Berliner, L. J., Reuben, J., Eds.; Plenum: New York, 1989; Vol. 8, p 77.
- (19) Kowert, B. A. *J. Phys. Chem.* **1981**, *85*, 229.
- (20) Budil, D. E.; Earle, K. A.; Freed, J. H. *J. Phys. Chem.* **1993**, *97*, 1294.
- (21) Kar, L.; Ney-Ignér, E.; Freed, J. H. *Biophys. J.* **1985**, *48*, 569.
- (22) Shin, Y. K.; Freed, J. H. *Biophys. J.* **1989**, *56*, 1093.
- (23) More, J. J.; Garbow, B. S.; Hillstrom, K. F. *Users' Guide for MINPACK-1*, publication ANL 80-74, National Technical Information Service: Springfield, VA, 1980.
- (24) The  $\rho_y$  vs  $\rho_x$  curves calculated from the full slow-motional theory do deviate appreciably from linearity for large anisotropies, i.e.,  $\rho_{x,y} > 10$  or  $\rho_{x,y} < 0.1$  about appropriate axes. Under these conditions, the secular spectral densities related to the hf tensor can no longer be neglected with respect to the g tensor spectral densities, an approximation that was made in the derivation of the linear AVE for  $A/B$ .<sup>20</sup> For very anisotropic motions, one should use a more general form of the AVE that can be derived from the expressions given in ref 20. Also, the methods of ref 20 do allow for the derivation of an AVE that includes a diffusion tilt angle, although the expressions become somewhat complicated in this case.
- (25) Goldman, S. A.; Bruno, G. V.; Polnaszek, C. F.; Freed, J. H. *J. Chem. Phys.* **1972**, *56*, 716.
- (26) Millhauser, G. L.; Freed, J. H. *J. Chem. Phys.* **1984**, *81*, 37; **1986**, *85*, 63.
- (27) Millhauser, G. L.; Gorcester, J.; Freed, J. H. In *Electronic Magnetic Resonance of the Solid State*; Weil, J. A., Ed.; Canadian Society for Chemistry: Ottawa, **1987**, p 571.
- (28) Polimeno, A.; Freed, J. H. *Chem. Phys. Lett.* **1990**, *174*, 338, 481; *Adv. Chem. Phys.* **1993**, *83*, 89.
- (29) Lamb, H. *Hydrodynamics*; Dover: New York, 1943.
- (30) Marriott, T. B.; Birrell, G. B.; Griffith, O. H. *J. Am. Chem. Soc.* **1975**, *97*, 627.
- (31) Zare, R. N. *Angular Momentum*; Wiley-Interscience: New York, 1988.
- (32) Bulthuis, J.; Plomp, L. *J. Phys. (Paris)* **1990**, *51*, 2581.